Multiple-Edge XAS Studies of Cyanide-Bridged Iron−Copper Molecular Assemblies Relevant to Cyanide-Inhibited Heme−Copper Oxidases Using Four-Body Multiple-Scattering Analysis

Hua Holly Zhang,[†] Adriano Filipponi,[§,⊥] Andrea Di Cicco,[‡,#] Michael J. Scott,[‖] R. H. Holm,*,[‖] Britt Hedman,*,[‡] and Keith O. Hodgson*,[†,‡]

Contribution from the Department of Chemistry, Stanford University, Stanford, California 94305, European Synchrotron Radiation Facility, B.P. 220, F-38043 Grenoble, France, Stanford Synchrotron Radiation Laboratory, Stanford University, Stanford, California 94309, and Department of Chemistry, Harvard University, Cambridge, Massachusetts 02138

Received September 19, 1996[⊗]

Abstract: A pair of cyanide-bridged iron−copper molecular assemblies relevant to cyanide-inhibited heme−copper oxidases has been studied by X-ray absorption spectroscopy at both Fe and Cu K-edges. These two complexes, [(py)(OEP)Fe−CN−Cu(Me₆tren)]²⁺ (**2**) and [(py)(OEP)Fe−CN−Cu(TIM)]²⁺ (**3**), contain a unique four-body Fe−C−N−Cu bridge with an Fe−C−N angle of 179°. They, however, differ significantly in the Cu−N−C angle (174° in **2** and 147° in **3**). These two complexes provide the opportunity to study long-range multiple scattering (MS) interactions between the Fe and the Cu centers. We have calculated theoretical four-body MS signals for the bridge configuration and other four-body pathways in the structures, and performed least-squares fittings of the theoretical signals to the experimental data using the GNXAS programs. A strong long-range Fe···Cu interaction (4.94 Å) has been observed from both the Fe and Cu K-edge data for **2**. GNXAS analysis shows that this long-range interaction is attributed to the MS amplitude enhancement from the linear four-body Fe−C−N−Cu configuration. This interaction is not observable from the Fe and Cu K-edge data for **3** where the angle deviates significantly from linearity. An angle-dependence study of MS effects on the Cu−N−C angle shows that there is a large enhancement of MS intensity when the angle approaches linearity, and that this MS effect is negligible when the angle is below ∼160°. Essentially no Fe−Cu interaction is detectable for a configuration with such an angle. Comparisons with three-body MS effects found in Fe−O/O(H)−Cu bridged systems are made. The significance of the findings of this study to the structural definition of the binuclear center in the cyanide-inhibited heme-copper oxidases is discussed.

Introduction[1]

We are engaged in extensive synthetic, structural, and spectroscopic investigations of heme-based molecular assemblies containing the unsupported bridges Fe^{III}−X−Cu^{II} with X = O^{2-},[2−5] OH$^-$,[3−5] RCO₂$^-$,[5,6] and CN$^-$.[7−10] These molecules are intended as actual or potential analogues of the oxidized

binuclear heme a_3−Cu$_B$ site in the superfamily of heme-copper respiratory oxidases.[11] Karlin and co-workers have also prepared and examined oxo- and hydroxo-bridged Fe^{III}Cu^{II} systems.[12] Dioxygen is bound, activated, and reduced at the binuclear site, whose existence—albeit without identification of bridging ligands—has been confirmed for two oxidases by protein crystallography.[13,14] In their oxidized and reduced forms, the oxidases bind certain exogenous anions, among them cyanide.[15−18] Binding of cyanide causes heme a_3 to assume a low-spin six-coordinate state, and alters the magnetic coupling from antiferromagnetic to ferromagnetic with attendant stabilization of an integer-spin ground state.[17,18] There is general consensus that the cyanide ion enters the binuclear site, blocks

---

* To whom correspondence should be addressed.
† Department of Chemistry, Stanford University.
§ European Synchrotron Radiation Facility.
‡ Stanford Synchrotron Radiation Laboratory, Stanford University.
‖ Harvard University.
⊥ Permanent address: Dipartimento di Fisica, Università degli Studi dell' Aquila, Via Vetoio, 67010 Coppito, L'Aquila, Italy.
Permanent address: Dipartimento di Matematica e Fisica, Università degli Studi di Camerino, Via Madonna delle Carceri, 62032 Camerino (MC), Italy.

(1) Abbreviations: EXAFS, extended X-ray absorption fine structure; FT, Fourier transform; GNXAS, *n*-body distribution function (g$_n$) and X-ray absorption spectroscopy; Me₆tren, tris(2-(dimethylamino)ethylamine; 1-MeIm, 1-methylimidazole; Me₅dien, 1,1,4,7,7-pentamethyldiethylenetriamine; MS, multiple scattering; py, pyridine; OEP, octaethylporphyrinate(2−); SS, single scattering; TIM, 2,3,9,10-tetramethyl-1,4,8,11-tetraazatetradeca-1,3,8,10-tetraene; XAS, X-ray absorption spectroscopy.
(2) Lee, S. C.; Holm, R. H. *J. Am. Chem. Soc.* **1993,** *115,* 5833, 11789.
(3) Scott, M. J.; Zhang, H. H.; Lee, S. C.; Hedman, B.; Hodgson, K. O.; Holm, R. H. *J. Am. Chem. Soc* **1995,** *117,* 568.
(4) Zhang, H. H.; Filipponi, A.; Di Cicco, A.; Lee, S. C.; Scott, M. J.; Holm, R. H.; Hedman, B.; Hodgson, K. O. *Inorg. Chem.* **1996,** *35,* 4819.
(5) Kauffmann, K.; Goddard, C. A.; Zang, Y.; Holm, R. H.; Münck, E. *Inorg. Chem.* In press.
(6) Scott, M. J.; Goddard, C. A.; Holm, R. H. *Inorg. Chem.* **1996,** *35,* 2558.

(7) Lee, S. C.; Scott, M. J.; Kauffmann, K.; Münck, E.; Holm, R. H. *J. Am. Chem. Soc.* **1994,** *116,* 401.
(8) Scott, M. J.; Lee, S. C.; Holm, R. H. *Inorg. Chem.* **1994,** *33,* 4651.
(9) Scott, M. J.; Holm, R. H. *J. Am. Chem. Soc.* **1994,** *116,* 11357.
(10) Gardner, M. T.; Deinum, G.; Kim, Y.; Babcock, G. T.; Scott, M. J.; Holm, R. H. *Inorg. Chem.* **1996,** *35,* 6878.
(11) (a) Babcock, G. T.; Wikström, M. *Nature* **1992,** *356,* 301. (b) Malmström, B. *Acc. Chem. Res.* **1993,** *26,* 332.
(12) (a) Karlin, K. D.; Nanthakumar, A.; Fox, S.; Murthy, N. N.; Ravi, N.; Huynh, B. H.; Orosz, R. D.; Day, E. P. *J. Am. Chem. Soc.* **1994,** *116,* 4753. (b) Fox, S.; Nanthakumar, A.; Wikström, M.; Karlin, K. D.; Blackburn, N. J. *J. Am. Chem. Soc.* **1996,** *118,* 24.
(13) Iwata, S.; Ostermeier, C.; Ludwig, B.; Michel, H. *Nature* **1995,** *376,* 660.
(14) Tsukihara, T.; Aoyama, H.; Yamashita, E.; Tomizaki, T.; Yamaguchi, H.; Shinzawa-Itoh, K.; Nakashima, R.; Yaono, R.; Yoshikawa, S. *Science* **1995,** *269,* 1069; **1996,** *272,* 1136.

oxygen binding, and hence prevents the reaction $O_2 + 4H^+ + 4e^- \rightarrow 2H_2O$.

As noted earlier,[9] there are three reasonable modes of cyanide binding in the oxidized form: (i) exclusive binding at Cu(II) or Fe(III); (ii) tight binding at one metal, with the terminal atom weakly interacting with the other metal or with a proton in a hydrogen bond; and (iii) formation of a tight linear or nonlinear [Fe^{III}−CN−Cu^{II}] bridge. Analogues of (i) devolve to rather simple heme− or Cu(II)−cyanide complexes, several examples of which exist and include molecules recently prepared by us.[8,9] We do not favor this mode because the cyanide stretching frequencies of Cu^{II}−CN and (heme)Fe^{III}−CN groups[8-10] are lower than those observed for the cyanide-treated oxidases which are typically in the range of $\nu_{CN} = 2146$−2152 cm^{-1}.[15b,e,g] Given the affinity of oxidized hemes for cyanide, under model (i) a Fe^{III}−CN interaction is expected, and for the complex [Fe(1-MeIm)(OEP)(CN)], a ν_{CN} of 2129 cm^{-1} is observed.[10] Binding mode (ii) involves weak interactions at the nitrogen atom. Based on our vibrational analysis of bridge unit **1** in structurally

1
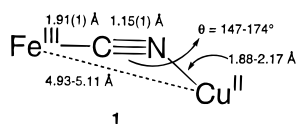
characterized model complexes and the slight (3 cm^{-1}) shift of the preceding heme complex in a hydrogen-bonding solvent,[10] we regard this mode as unlikely. Binding mode (iii) implicates the bridge unit **1**, which we have prepared and crystallographically demonstrated in some seven different molecules of the general type [(py)(OEP) Fe^{III} −CN−Cu^{II}LL′]$^{1+,2+}$, where L is a tridentate or tetradentate nitrogeneous ligand and L′ is a unidentate neutral or anionic ligand (absent when L is tetradentate).[7-9] In bridge **1**, the Fe−C and C−N bond distances are essentially invariant and average values are shown; in addition, the mean Fe−C−N angle is 178(2)°. However, both the Cu−N distance and the Cu−N−C angle θ are pliable and can be empirically varied over the indicated ranges—and with them the Fe···Cu separation—by the use of different ligands L/L′. The ν_{CN} values for the oxidases are covered by the range $\nu_{CN} \approx 2140$−2185 cm^{-1} of the synthetic complexes, whose frequencies depend on the interplay between θ and the Cu−N bond length.[9] Further, bridge **1** in synthetic complexes propagates a spin-coupling interaction leading to an integer-spin ground state. Consequently, we favor binding mode (iii) in the enzymes.

As an overall goal, we seek a molecular description of cyanide toxicity by demonstrating as directly as possible the mode of cyanide binding in inhibited oxidases. Synthetic bridged molecular assemblies of known structure provide indispensable reference points for this problem when pursued by various spectroscopic methods including XAS. Our first complete

EXAFS study of [Fe^{III}−X−Cu^{II}] bridges targeted on the oxo and hydroxo cases.[4] These complexes, [(OEP)Fe−O−Cu(Me$_6$tren)]$^{1+}$ and [(OEP)Fe−(OH)−Cu(Me$_5$tren)(OClO$_3$)]$^{1+}$, constitute a useful pair with which we were able to observe and quantitatively analyze a strong bridge-angle dependence of MS effects at both the Fe and Cu K-edges. This study employed a correlated three-body MS analysis (with the GNXAS program suite[19-22]) that gave rise to accurate determination of distances and angles for these systems. A similar study using a different pair, in which the structure of the hydroxo member was determined by EXAFS, has been reported.[12b]

In contrast, bridges of the type [M−X−Y−M′] at or near linearity may require treatment of a correlated *four-body* MS pathway. An understanding of these more complicated MS effects is necessary if the putative cyanide bridge of type **1** in binuclear oxidase sites is to be successfully probed by EXAFS. In this investigation, we have undertaken EXAFS analysis of the pair of molecular assemblies [(py)(OEP)Fe−CN−Cu(Me$_6$tren)]$^{2+}$ (**2**)[7,8] and [(py)(OEP)Fe−CN−Cu(TIM)]$^{2+}$ (**3**).[9] This investigation is the first application to molecular inorganic complexes of the newest version of GNXAS that allows for four-body MS treatments and provides an efficient description of four-body configurations. As with the oxo/hydroxo-bridged pair, complexes **2** and **3** can be studied at both the Fe and Cu edges (including multiple-edge refinement[4,23]). We have hence examined the long-range interactions between the two metals through the Fe−C−N−Cu configuration and determined the extent to which these interactions are significant from the EXAFS point of view. We note that Penner-Hahn and co-workers have studied linear Cu−C−N−Cu systems relevant to organocuprate reagents by Cu K-edge EXAFS.[24] Using FEFF[25] MS calculations, they have shown a Cu···Cu interaction in the outer shell at ~5.0 Å. Similar metal−metal interactions have also been examined by FEFF on a Mo complex with a linear four-body Mo−N≡N−Mo configuration.[26] In neither of these cases was the four-body interaction treated as fully correlated assemblies.

For the study reported herein, complexes **2** (174°) and **3** (147°) were selected because they are limiting in Cu−N−C bridge angle among the set of seven structurally defined complexes described earlier. This large difference in bridge geometry affords the unique opportunity to investigate the angular sensitivity of the four-body MS effects and to compare the results with those from the three-body oxo- and hydroxo-bridge cases.[4] At the same time, a comparison of GNXAS-determined structural parameters with the known crystallographic values provides a means to evaluate the accuracy of the method in treating four-body problems. We have also performed a statistical analysis of errors using contour plots[22,27] to identify correlations among fitting parameters and to establish the error limits.

(15) (a) Baker, G. M.; Noguchi, M.; Palmer, G. *Biochemistry* **1987**, *32*, 7855. (b) Yoshikawa, S.; Caughey, W. S. *J. Biol. Chem.* **1990**, *265*, 7945. (c) Surerus, K. K.; Oertling, W. A.; Fan, C.; Gurbiel, R. J.; Einarsdóttir, O.; Antholine, W. E.; Dyer, R. B.; Hoffman, B. M.; Woodruff, W. H.; Fee, J. A. *Proc. Natl. Acad. Sci. USA* **1992**, *89*, 3195. (d) Caughey, W. S.; Dong, A.; Sampath, V.; Yoshikawa, S.; Zhao, X. J. *Bioenerg. Biomemb.* **1993**, *25*, 81. (e) Tsubaki, M.; Yoshikawa, S. *Biochemistry* **1993**, *32*, 164. (f) Li, W.; Palmer, G. *Biochemistry* **1993**, *32*, 1833. (g) Tsubaki, M.; Mogi, T.; Anraku, Y.; Hori, H. *Biochemistry* **1993**, *32*, 6065.

(16) Palmer, G. *Bioenerg. Biomemb.* **1993**, *25*, 145.

(17) (a) Eglinton, D. G.; Johnson, M. K.; Thomson, A. J.; Gooding, P. E.; Greenwood, C. *Biochem. J.* **1980**, *191*, 319. (b) Thomson, A. J.; Johnson, M. K.; Greenwood, C.; Gooding, P. E. *Biochem. J.* **1981**, *193*, 687.

(18) (a) Kent, T. A.; Münck, E.; Dunham, W. R.; Filter, W. F.; Findling, K. L.; Yoshida, T.; Fee, J. A. *J. Biol. Chem.* **1982**, *257*, 12489. (b) Kent, T. A.; Young, L. J.; Palmer, G.; Fee, J. A.; Münck, E. *J. Biol. Chem.* **1983**, *258*, 8543.

(19) Westre, T. E.; Di Cicco, A.; Filipponi, A.; Natoli, C. R.; Hedman, B.; Solomon, E. I.; Hodgson, K. O. *J. Am. Chem. Soc.* **1994**, *116*, 6757.

(20) Westre, T. E.; Di Cicco, A.; Filipponi, A.; Natoli, C. R.; Hedman, B.; Solomon, E. I.; Hodgson, K. O. *J. Am. Chem. Soc.* **1995**, *117*, 1566.

(21) Filipponi, A.; Di Cicco, A.; Natoli, C. R. *Phys. Rev. B* **1995**, *52*, 15122.

(22) Filipponi, A.; Di Cicco, A. *Phys. Rev. B* **1995**, *52*, 15135.

(23) Di Cicco, A. *Phys. Rev. B* **1996**, *53*, 6174.

(24) Stemmler, T. L.; Barnhart, T. M.; Penner-Hahn, J. E.; Tucker, C. E.; Knochel, P.; Böhme, M.; Frenking, G. *J. Am. Chem. Soc.* **1995**, *117*, 12489.

(25) (a) Rehr, J. J.; Mustre de Leon, J.; Zabinsky, S. I.; Albers, R. C. *J. Am. Chem. Soc.* **1991**, *113*, 5135. (b) Rehr, J. J.; Albers, R. C.; Zabinsky, S. I. *Phys. Rev. Lett.* **1992**, *69*, 3397.

(26) Laplaza, C. E.; Johnson, M. J. A.; Peters, J.; Odom, A. L.; Kim, E.; Cummins, C. C.; George, G. N.; Pickering, I. J. *J. Am. Chem. Soc.* **1996**, *118*, 8623.

(27) Filipponi, A. *J. Phys.: Condens. Matter* **1995**, *7*, 9343.

2472   *J. Am. Chem. Soc., Vol. 119, No. 10, 1997*

Zhang et al.

Experimental Section

Sample Preparation and EXAFS Data Collection and Reduction. The compounds **[2]**(ClO$_4$)$_2$[7,8] and **[3]**(PF$_6$)$_2$[9] were prepared as described. Solid samples were ground to a fine powder and diluted with boron nitride under a dry dinitrogen atmosphere in a glovebox. The powder samples were transferred into a 1-mm-thick slotted Al spacer, pressed into a fine pellet, and sealed between 63.5-μm Mylar windows. Upon removal from the glovebox, the samples were immediately frozen in liquid nitrogen and kept at this temperature prior to measurements.

Transmission X-ray absorption spectroscopic data were recorded at the Stanford Synchrotron Radiation Laboratory (SSRL) on unfocused beamline 7−3, with ring conditions 3.0 GeV, 60 mA. Both the Fe and Cu K-edge data were measured using a Si(220) double-crystal monochromator, and the samples were maintained at a constant temperature of 10 K by an Oxford Instruments CF1208 continuous-flow liquid-helium cryostat. Internal energy calibration was performed by placing an Fe or Cu foil between the second and the third nitrogen-filled ionization chambers. The first inflection point of the foil spectra was assigned to be 7111.2 eV for Fe and 8980.3 eV for Cu. The data represent averages of multiple scans (6−11), and these averaged raw data, without background subtraction, were input into the GNXAS program and analyzed.

GNXAS Data Analysis. An expanded version of the integrated EXAFS package GNXAS was used to analyze the data.[21,22] Its fitting methodologies and statistical treatment of errors for inorganic complexes have been explained in detail in previous publications.[4,19,20] For the study reported herein, a model cluster up to a distance cutoff of 5.5 Å was generated using the crystallographic coordinates of **2**[7] and **3**[9], and the two- and three-body configurations in each cluster were identified with a frequency tolerance of 0.05 Å. In practice, this means that the porphyrin contribution has 4*mm* symmetry. Phase shifts were calculated using the standard muffin-tin approximation, and individual SS and MS EXAFS signals for selected two-body and three-body configurations were then generated. A model EXAFS spectrum was built by combining all the individual signals and an appropriate background. This model EXAFS spectrum was refined against the experimental absorption data using a least-squares minimization procedure that varied structural and nonstructural parameters.[4,19,20] As described earlier,[4] GNXAS refines the spline parameters simultaneously with the structural parameters.

The parameters used are explained as follows. The nonstructural parameters included in the fitting were E_0 (core ionization threshold), S_0^2 (many-body amplitude reduction factor), E_r (experimental resolution), and Γ_c (core-hole lifetime). The first three were varied during the refinement (E_r was slightly varied around the known energy resolutions), and Γ_c was kept fixed to tabulated values.[28] The structural parameters varied for a two- or three-body signal have been explained in detail earlier.[4] Specifically, they were the bond distance (R) and the bond variance (σ_R^2) for a two-body signal, the two shorter bond distances (R_1 and R_2), the intervening angle (θ), and the six covariance matrix elements for a three-body signal. The coordination numbers were fixed at the known crystallographic values. For a linear three-body signal, the angle of 180° was fixed and the angle variance (δ_θ^2) was used as a way of evaluating the deviation of the fitting results from the crystallographical values as previously discussed.[4] The quality of the fits was determined by the goodness-of-fit parameters, R,[20] and by careful inspection of the EXAFS residuals and their FTs.

The geometrical description of a four-body configuration is much more complicated. For a generic four-body chain topology, $o-i-j-k$, where o is the photoabsorber, the geometry is established by the following six parameters: R_{o-i}, R_{i-j}, θ_{oij}, R_{j-k}, θ_{ijk}, and ψ (the dihedral angle defining the spatial orientation of the three bonds). Thermal and static disorder of the configuration is taken into account through 21 parameters belonging to a 6 × 6 symmetric covariance matrix: three bond variances, three angle variances, and 15 off-diagonal matrix elements representing the correlations between pairs of bonds and/or angles. Thus, a total of 27 structural parameters is needed to fit a four-body configuration. However, for the two structures studied herein, the increase in the number of fitting parameters was actually much

smaller than 27 when a four-body signal was included. Specifically, the four-body pathways contained some of the three-body pathways used in the fit; therefore, the same parameters describing these three-body pathways were used in the four-body case. Further, the important four-body configurations in the two structures are collinear or nearly planar. In these special cases, the covariance matrix contains a reduced number of terms. For a planar structure, the dihedral angle ψ reaches an extreme and covariance parameters involving ψ vanish. For a collinear structure, any bond or angle correlation with $\theta = 180°$ is zero. In particular, the covariance matrix of the Fe−C−N−Cu collinear four-body configuration (both collinear and planar) contains only 8 terms: $\sigma_{R_1}^2$, $\sigma_{R_2}^2$, $\sigma_{R_3}^2$, ρ_{R_1,R_2}, ρ_{R_2,R_3}, ρ_{R_1,R_3}, $\sigma_{\theta_1}^2$, and $\sigma_{\theta_2}^2$. For the other four-body signals used in the fit (their structures being planar but not linear), the covariance matrix has 7 more terms in addition to the 8 terms described above. They are the correlations with the two nonzero angles, θ_1 and θ_2: ρ_{R_1,θ_1}, ρ_{R_1,θ_2}, ρ_{R_2,θ_1}, ρ_{R_2,θ_2}, ρ_{R_3,θ_1}, ρ_{R_3,θ_2}, and ρ_{θ_1,θ_2}.

In the case of **2**, the number of the fitting parameters was further reduced by using a simultaneous multiple-edge fitting of the Fe and Cu K-edge data. As detailed in earlier publications,[4,23] such analysis allows common pathways to be constrained to be the same, which in this case are the parameters of the Fe−C−N−Cu structure. Only one set of these parameters was introduced and refined against *both* the Fe and Cu K-edge data. In the case of **3**, single-edge fits were performed because the Fe and Cu data did not contain overlapped information as those seen in **2**; neither metal could be seen from the data of the other one (see results and discussion section for details).

For the final fits, the total number of the fitting parameters for the multiple-edge result of **2** was 50. Due to a limitation in the dimensioning of the program, ρ_{R_1,R_3}, ρ_{R_1,θ_2}, ρ_{R_3,θ_1}, and ρ_{θ_1,θ_2} of the four-body signal from the porphyrin contribution were set to zero and weak signals were excluded. The total number of the fitting parameters for the single-edge fit of the Fe and Cu K-edge data of **3** were 40 and 46, respectively. It is useful to include here the number of independent data points in the EXAFS spectrum for comparison. Using the formula provided by Stern,[29] the number of independent points were 74 for **2** and 38 and 36 for the Fe and Cu K-edges for **3**. The relatively large number of the fitting parameters in **3** may result in higher errors in the fitting results.

Throughout the paper, an effective signal from a three-body configuration $o-i-j$ (where o is the photoabsorber) includes contributions from a two-body SS term $\gamma^{(2)}$ (associated with the most distant atom, $o\cdots j$) and a three-body MS term $\gamma^{(3)}$ ($o-i-j$).[21] Similarly, an effective 4-body signal $o-i-j-k$ (where o is the photoabsorber) includes $\gamma^{(2)}$ ($o\cdots k$), two 3-body MS terms $\gamma^{(3)}$ ($o-i\cdots k$ and $o\cdots j-k$), and one 4-body MS term $\gamma^{(4)}$ ($o-i-j-k$).

Results and Discussion

Fe K-Edge Analysis of [(py)(OEP)Fe−CN−Cu(Me$_6$tren)]$^{2+}$ (2) and [(py)(OEP)Fe−CN−Cu(TIM)]$^{2+}$ (3). The structures of **2** and **3**, set out in Figure 1, are quite similar from the Fe point of view. Consequently, the two fit results are discussed together for comparison. The k^3-weighted EXAFS data and the corresponding FTs for **2** and **3** are presented in Figures 2 and 3. A careful inspection of the FTs shows strong similarity between **2** and **3** up to 4 Å. Beyond this point, **3** is essentially featureless whereas **2** has a significant peak at ∼4.6 Å and its EXAFS signal exhibits more features, especially in the higher k region (above 9 Å^{-1}).

The individual EXAFS contributions required for a good fit for **2** and **3** are given in Figures 4 and 5, respectively. Both first-shell fits required the contributions from the carbon atom of the cyanide bridge, Fe−C(1), and from the five nitrogen atoms of the porphyrin and pyridine ligands. The five nitrogen atoms in **2** contributed to one SS Fe−N(1) signal with a multiplicity of five. For **3**, however, a better fit was obtained when the axial nitrogen atom from the pyridine was treated as a separate SS signal, Fe−N(1b), from the other four nitrogens from the porphyrin, Fe−N(1a), as the Fe−N(1b) bond length

(28) Krause, M. O.; Oliver, J. H. *J. Phys. Chem. Ref. Data* **1979**, *8*, 329.

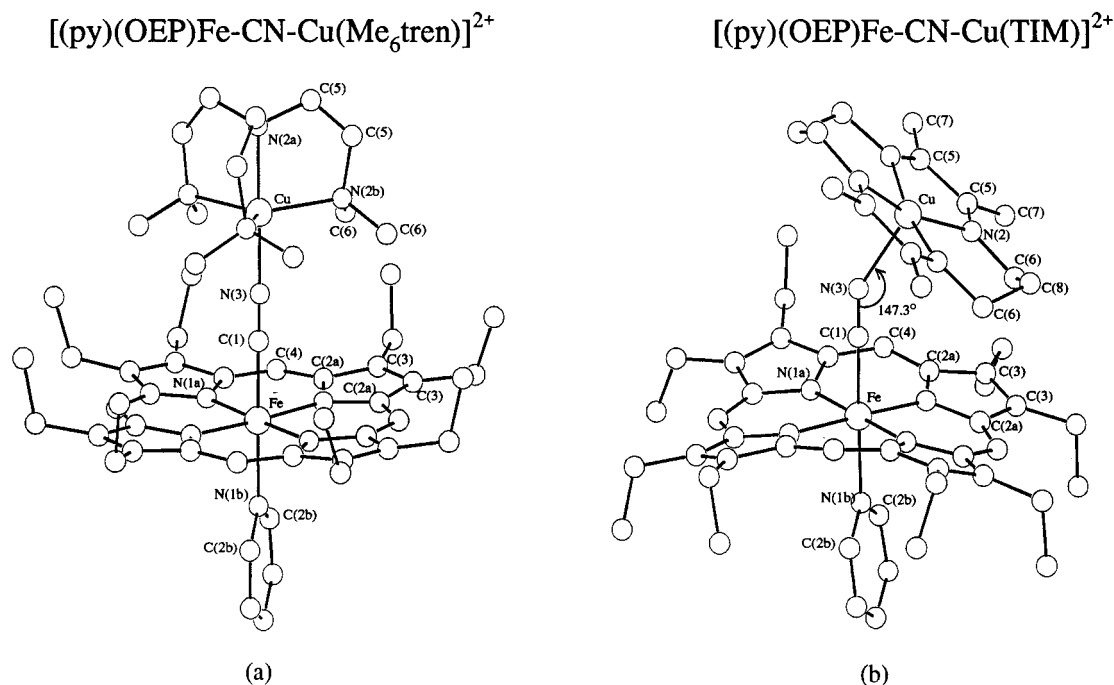(29) Stern, E. A. *Phys. Rev. B* **1993**, *48*, 9825.

$[(py)(OEP)Fe\text{-}CN\text{-}Cu(Me_6tren)]^{2+}$ $[(py)(OEP)Fe\text{-}CN\text{-}Cu(TIM)]^{2+}$

(a)   (b)

Figure 1. Structures of $[(py)(OEP)Fe−CN−Cu(Me_6tren)]^{2+}$ (**2**, a) and $[(py)(OEP)Fe−CN−Cu(TIM)]^{2+}$ (**3**, b) drawn from crystallographic coordinates;[7−9] key metric parameters are listed in Tables 1 and 2. The major difference between the two structures bearing significance in the EXAFS signal is the bridge structure **1**, being linear in **2** *vs* bent in **3**.

is 0.1 Å longer than the average Fe−N(1a) bond length, according to the crystallographic values. This also resulted in a different treatment of the 3-body MS contributions Fe−N(1)−C(2) for **2** and **3**, *i.e.* one Fe−N(1)−C(2) with a multiplicity of 10 for **2**, one Fe−N(1a)−C(2a) with a multiplicity of 8, and one Fe−N(1b)−C(2b) with a multiplicity of two for **3**. All the first-shell signals as well as the outer-shell contributions from the porphyrin and pyridine ligands fall in the range between 1.9 and 4.3 Å. The final fit shows that they well accounted for the FT features below ∼4 Å (Figure 3).

The major difference between **2** and **3** in the FT region of 4−5 Å is attributed to the difference in the long-range interactions between Fe and Cu, and the 4.6-Å feature in the FT of **2** can be well explained by a four-body Fe−C−N−Cu contribution. As seen in Figure 1, the four-atom bridge structure of **2** is essentially linear, with a Fe−C(1)−N(3) angle of 179° and a C(1)−N(3)−Cu angle of 174°. This linear four-body configuration greatly enhances the long-range interaction through the so-called focusing effect[19,30,31] which generates strong MS effects. The calculations show that the four-body EXAFS signal is quite strong and becomes more intense at higher k, which is typical of a metal−metal interaction (Figure 4). The bridge structure in **3**, on the other hand, is bent at the Cu end, with a Fe−C(1)−N(3) angle of 179° and a C(1)−N(3)−Cu angle of 147.3°. This angular change in the bridge structure substantially decreases the Fe−Cu MS contributions. Its EXAFS is so weak that it does not contribute in a statistically meaningful fashion. As a result, the Fe···Cu distance of 5.02 Å known from the crystal structure could not be fit to the data.

A breakdown of the 4.6-Å peak in **2** into its four components (Figure 3a, inset) gives an even more convincing illustration of this MS mechanism. A simple calculation indicates that the Fe···Cu two-body term $\gamma^{(2)}$ accounts for 7% of the total intensity, the two three-body MS terms $\gamma^{(3)}$, Fe···N(3)−Cu and Fe−C(1)···Cu, account for 20% and 23%, respectively, and the

four-body MS pathway $\gamma^{(4)}$, Fe−C(1)−N(3)−Cu, accounts for *50%*. Figure 6a displays the relative strengths of the EXAFS signals of the four components. It is evident that the linear four-body interaction $\gamma^{(4)}$ is the main contributor to the intense outer-shell feature. A fit without $\gamma^{(4)}$ increases the R value from 0.411×10^{-8} to 1.17×10^{-8} (multiple-edge fit), almost a factor of 3, and a high-frequency wave dominates in the EXAFS residual (see Figure 2b).

A comparison of the relative strengths of the individual components in the EXAFS of **2** with those of the nitrogenase MoFe protein[32] provides additional insight. In that case, a long-range interaction between Mo and Fe in the heteronuclear Mo−Fe−S cluster was observed at a distance of about 5 Å from the Mo K-edge data. It was found that this interaction originated from the Mo−Fe(1)−Fe(2) three-body configuration with a Mo−Fe(1)−Fe(2) angle of 152° and its EXAFS signal was enhanced by two heavy atoms, the intervening and backscattering Fe atoms. The fitting results showed a ∼3:2 ratio of SS *vs* MS contributions to the FT peak at ∼4.8 Å, indicating that the strong signal from Mo−Fe(1)−Fe(2) was more from a direct interaction between Mo and Fe(2) than a MS interaction through the three-body configuration. This is in sharp contrast to the effects for the linear four-body system of **2**.

We have previously published the GNXAS fits of the data for the linearly bridged $[(OEP)Fe^{III}−O−Cu^{II}(Me_6tren)]^{1+}$ *vs* the bent $[(OEP)Fe^{III}−(OH)−Cu^{II}(Me_5tren)(OClO_3)]^{1+}$ assemblies,[4] which demonstrated similar MS effects as a function of the bridge angle. These MS effects, however, are relatively short-ranged compared to that for the systems presented here; with one oxygen bridging between Fe and Cu, the Fe−Cu interaction was in the range of 3.5−3.8 Å. While the data for the oxo and the cyanide-bridged complex **2** display amplitude enhancement due to the linear configuration, the strong Fe−Cu MS interaction in **2** has been extended out to ∼5.0 Å. On the other hand, unlike the hydroxo complex whose Fe−O(H)−Cu EXAFS signal was

(30) Teo, B. K. *J. Am. Chem. Soc.* **1981**, *103*, 3990.
(31) Co, M. S.; Hendrickson, W. A.; Hodgson, K. O.; Doniach, S. *J. Am. Chem. Soc.* **1983**, *105*, 1144.

(32) Liu, H. I.; Filipponi, A.; Gavini, N.; Burgess, B. K.; Hedman, B.; Di Cicco, A.; Natoli, C. R.; Hodgson, K. O. *J. Am. Chem. Soc.* **1994**, *116*, 2418.
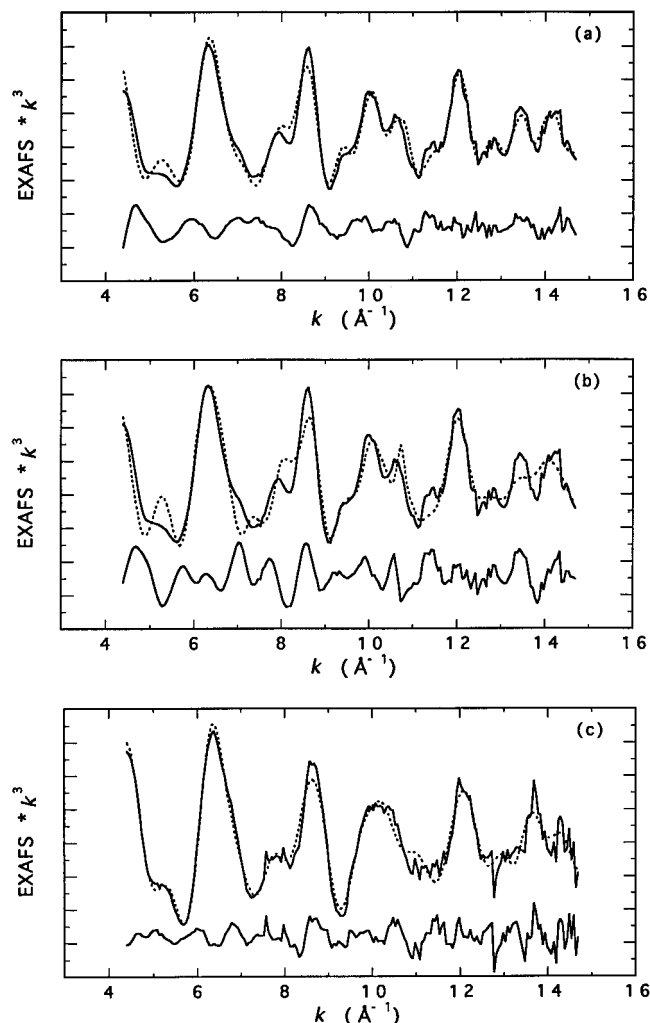
Figure 2. The experimental EXAFS data (—) *vs* the fit signal (···) of the Fe K-edge for the following: (a) [(py)(OEP)Fe−CN−Cu(Me₆-tren)]²⁺ (**2**), with the $\gamma^{(4)}$ MS contribution; (b) [(py)(OEP)Fe−CN−Cu(Me₆tren)]²⁺ (**2**), without the $\gamma^{(4)}$ MS contribution; (c) [(py)(OEP)Fe−CN−Cu(TIM)]²⁺ (**3**). The fit residual is also shown below the total signal. A high-frequency pattern in the residual is clearly seen in (b) when $\gamma^{(4)}$, the linear Fe−C(1)−N(3)−Cu four-body MS contribution, is not included in the fit. (The ordinate scale is 2.5 between two consecutive longer marks.)

weak yet significant to the fit, the data for the bent structure of **3**, with a similar bridge angle around 150°, required no Fe−C(1)−N(3)−Cu contribution to the fit. The long-range SS Fe···Cu falls off fast as the distance becomes longer (3.8 *vs* 5.0 Å).

In addition to the Fe−C(1)−N(3)−Cu four-body contribution, a successful fit also required a four-body contribution from the porphyrin ligand, Fe−N(1a)−C(2a)−C(3). Even though the pathway is not linear, the signal is significant as a result of the porphyrin-induced multiplicity of 8. However, this type of four-body signal receives a different set of contributions from its four components. While the linear four-body signal has a dominant $\gamma^{(4)}$ character and less than 10% $\gamma^{(2)}$ character, the porphyrin four-body signal has a more even distribution among $\gamma^{(2)}$, $\gamma^{(3)}$, and $\gamma^{(4)}$ (Figure 6b). This clearly demonstrates the mechanism by which the two types of four-body configurations contribute to the total EXAFS for these complex systems.

Cu K-Edge Analysis of [(py)(OEP)Fe−CN−Cu(Me₆tren)]²⁺ (2) and [(py)(OEP)Fe−CN−Cu(TIM)]²⁺ (3). The Cu fragments of the two structures are markedly different. Both have a five-coordinate Cu, but **2** is in a trigonal bipyramidal
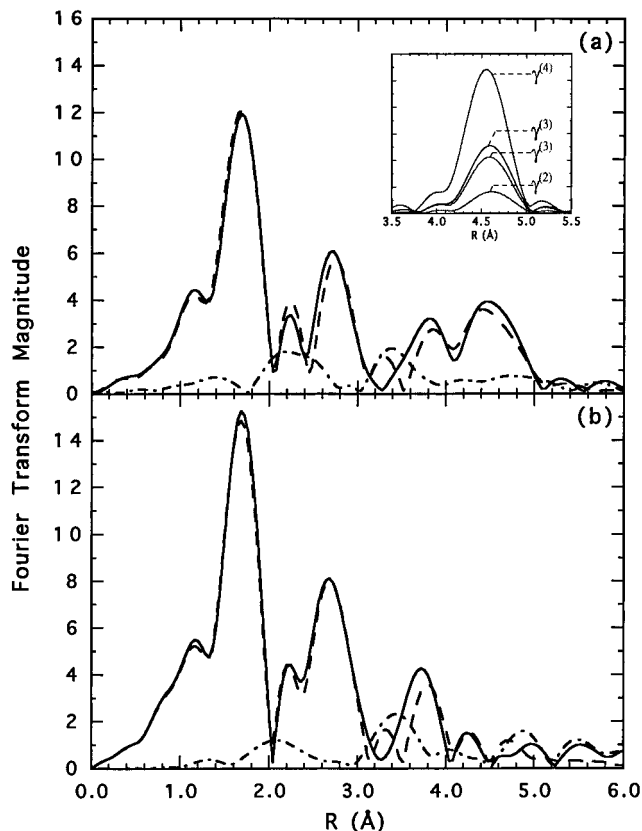

Figure 3. Non-phase-shift-corrected FTs of the experimental (—) *vs* the fit signals (- -) of the Fe K-edge EXAFS for the following: (a) [(py)(OEP)Fe−CN−Cu(Me₆tren)]²⁺ (**2**); (b) [(py)(OEP)Fe−CN−Cu(TIM)]²⁺ (**3**). The major difference between (a) and (b) is the 4.6-Å feature in (a), which is attributed to the linear bridge structure Fe−C(1)−N(3)−Cu. Inset: Components of the 4.6-Å FT feature. They originate from the four contributing pathways of the Fe−C−N−Cu structure, $\gamma^{(2)}$, $\gamma^{(3)}$, $\gamma^{(3)}$, and $\gamma^{(4)}$. Note the overwhelmingly strong $\gamma^{(4)}$ contribution (see text for discussion).
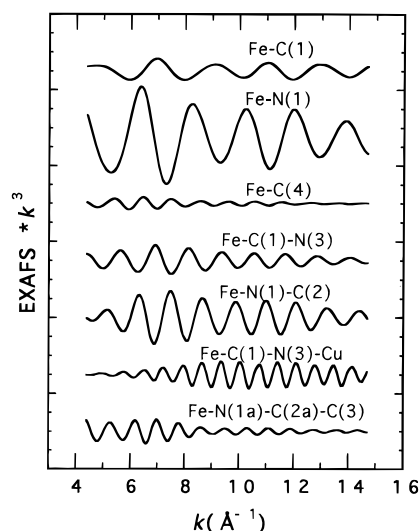

Figure 4. Individual EXAFS contributions of Fe K-edge fits for [(py)-(OEP)Fe−CN−Cu(Me₆tren)]²⁺ (**2**). Each signal is an effective signal, *i.e.* $\gamma^{(2)}$ and $\gamma^{(3)}$ combined for a three-body configuration and $\gamma^{(2)}$, $\gamma^{(3)}$, $\gamma^{(3)}$, and $\gamma^{(4)}$ combined for a four-body configuration. (The ordinate scale is 8 between two consecutive longer marks.)

environment while **3** has a nearly square pyramidal coordination. The comparison bearing significance in the EXAFS, however, comes from the bridge structure **1**. Crystallographic data show that the Cu−N(3)−C(1) angle decreases from 174° to 147° and the Cu−N(3) bond length increases from 1.90 to 2.17 Å upon
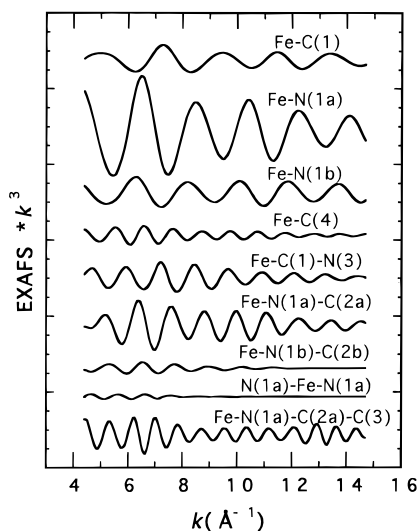
Cyanide-Bridged Iron—Copper Molecular Assemblies

J. Am. Chem. Soc., Vol. 119, No. 10, 1997 2475

Figure 5. Individual EXAFS contributions of Fe K-edge fits for [(py)-(OEP)Fe—CN—Cu(TIM)]$^{2+}$ (**3**). Each signal is an effective signal, *i.e.* $\gamma^{(2)}$ and $\gamma^{(3)}$ combined for a three-body configuration and $\gamma^{(2)}$, $\gamma^{(3)}$, $\gamma^{(3)}$, and $\gamma^{(4)}$ combined for a four-body configuration. (The ordinate scale is 8 between two consecutive longer marks.)
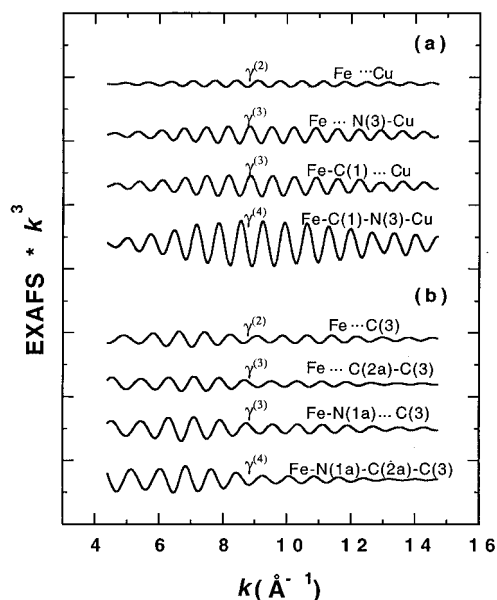
Figure 6. Relative Fe K-edge EXAFS strengths of the four contributing pathways in a four-body configuration for (a) the linear bridge Fe—C(1)—N(3)—Cu structure and (b) the Fe—N(1a)—C(2a)—C(3) structure in the porphyrin of **2**. While the four contributions in (b) are relatively equal in strength, $\gamma^{(4)}$ is the major contributor in (a). (The ordinate scale is 10 between two consecutive longer marks.)

passing from **2** to **3**. The changes in both the angle and the bond length result in drastic changes in the EXAFS and its FT, as observed in Figures 7 and 8.

As seen from the individual contributions shown in Figures 9 and 10, the shorter Cu—N(3) bond length in **2** generates stronger SS signals than the corresponding one in **3**. As a result, the Cu—N(3) signal in **2** with a multiplicity of one has almost the same intensity as the Cu—N(2b) signal having a multiplicity of three. The same effect can also be seen in the SS signal from the relatively short Cu—N(2a) bond. Because there is no dominant first-shell signal in **2** and the three first-shell signals interfere with each other destructively (as evidenced by the unusual EXAFS oscillation at low *k* in the total EXAFS, Figure 7), the first-shell FT peaks are not well resolved and overlap with the second-shell peak, resulting in broad FT peaks of small
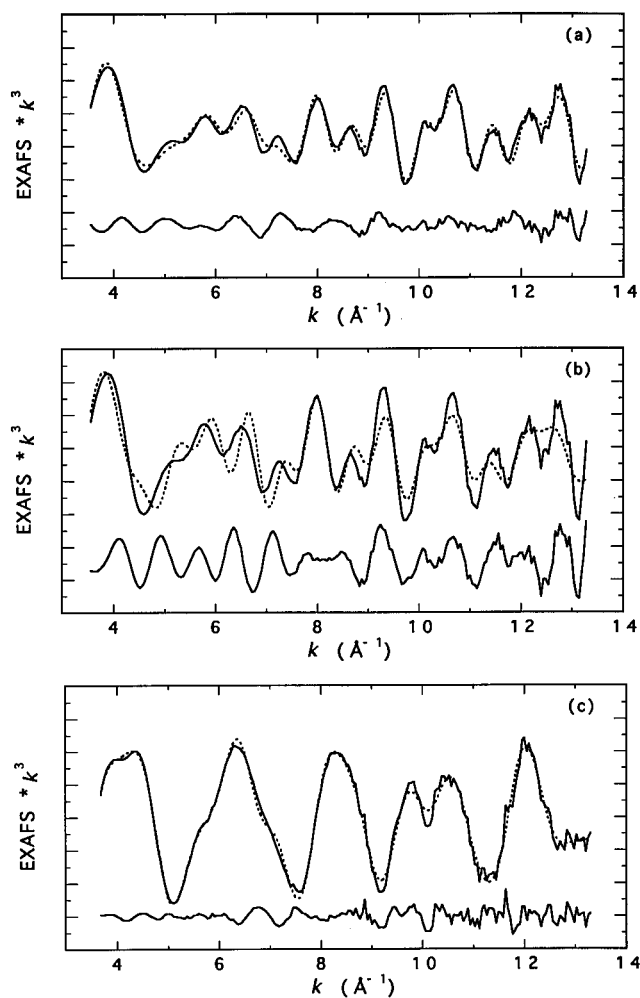

Figure 7. The experimental EXAFS data (—) *vs* the fit signal (···) of the Cu K-edge for the following: (a) [(py)(OEP)Fe—CN—Cu(Me$_6$-tren)]$^{2+}$ (**2**), with the $\gamma^{(4)}$ MS contribution; (b) [(py)(OEP)Fe—CN—Cu(Me$_6$tren)]$^{2+}$ (**2**), without the $\gamma^{(4)}$ MS contribution; (c) [(py)(OEP)Fe—CN—Cu(TIM)]$^{2+}$ (**3**). The fit residual is also shown below the total signal. (The ordinate scale is 2.5 between two consecutive longer marks.)

magnitude below ~3.2 Å (Figure 8a). For **3**, the intensity of the two first-shell signals follows the general rule in that the Cu—N(2) signal with a multiplicity of four is stronger than the singular Cu—N(3) signal (Figure 10). The overwhelmingly strong Cu—N(2) signal essentially dictates the position and the magnitude of the first-shell FT peak.

As with the Fe K-edge data, the change in the bridge angle at the Cu end brings about the most significant difference between **2** and **3**. The strong Cu—Fe MS interaction through the linear configuration in **2** contributes significantly to a distinctive FT peak at ~4.6 Å (Figure 8a). The unusually small magnitude of the first-shell peak makes this outer-shell feature appear even more dramatic. A fit excluding the Cu—N(3)—C(1)—Fe $\gamma^{(4)}$ signal resulted in a clear high-frequency oscillation in the residual (see Figure 7b). It should be noted that in some cases where the fit does not include a major EXAFS contribution, this can lead to a change in the background subtracted EXAFS data (as the spline is varied in the refinement) and hence a small difference in appearance from fit-to-fit. Such is the case when comparing the data and fits shown in Figures 7a and 7b where the major contribution of the 4-body signal was omitted in Figure 7b. The metrical results for both fits were quite similar, in both cases agreeing well with the crystallographic values. However, there was significant change (up
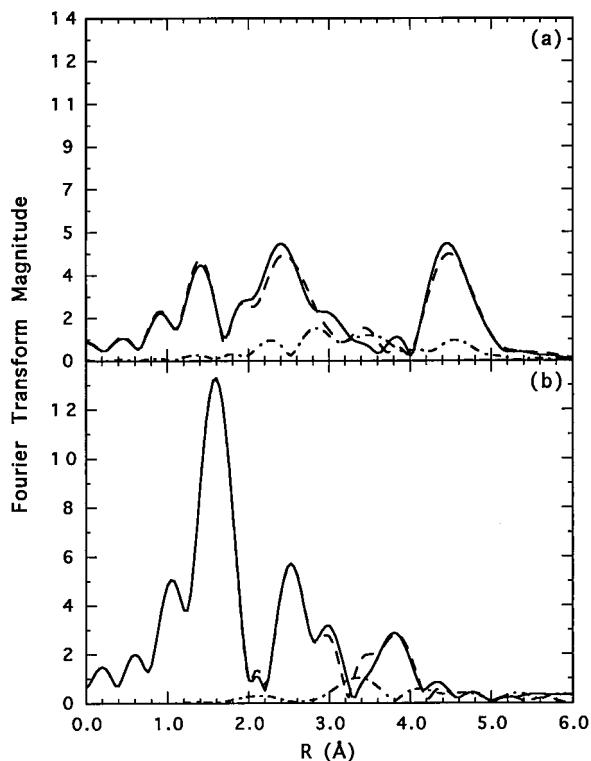
Figure 8. Non-phase-shift-corrected FTs of the experimental (—) *vs* the fit signals (- -) of the Cu K-edge EXAFS for the following: (a) [(py)(OEP)Fe−CN−Cu(Me₆tren)]²⁺ (**2**); (b) [(py)(OEP)Fe−CN−Cu(TIM)]²⁺ (**3**). As for the Fe K-edge data, the 4.6-Å feature in (a), due to the linear bridge structure Fe−C−N−Cu, is remarkably strong.
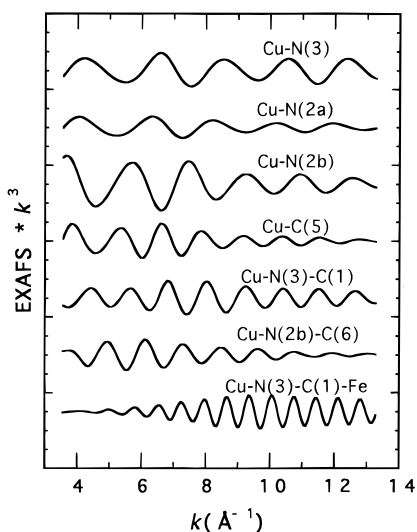

Figure 9. Individual EXAFS contributions of Cu K-edge fits for [(py)-(OEP)Fe−CN−Cu(Me₆tren)]²⁺ (**2**). Each signal is an effective signal, *i.e.* $\gamma^{(2)}$ and $\gamma^{(3)}$ combined for a three-body configuration and $\gamma^{(2)}$, $\gamma^{(3)}$, $\gamma^{(3)}$, and $\gamma^{(4)}$ combined for a four-body configuration. (The ordinate scale is 8 between two consecutive longer marks.)

to 2-fold) in some of the bond/angle variances as the fit attempted to compensate for the loss of this strong signal.

With the strong four-body MS contribution absent in its FT, the signal in **3** that is worth noting is the four-body contribution from Cu−N(2)−C(5)−C(7), which accounts for the outer-shell FT peak at 3.8 Å (Figure 8b). As at the Fe K-edge for the rigid porphyrin ligand, the regularity of the Cu fragment in **3** produces a Cu−N(2)−C(5)−C(7) signal with a multiplicity of four; therefore, it is a significant contributor to the total EXAFS. Among the four components of the four-body configuration, $\gamma^{(4)}$ amounts to 29% of the total intensity. Various fits showed
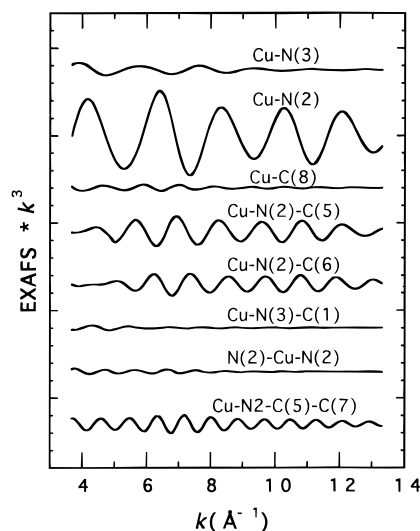

Figure 10. Individual EXAFS contributions of Cu K-edge fits for [(py)-(OEP)Fe−CN−Cu(TIM)]²⁺ (**3**). Each signal is an effective signal, *i.e.* $\gamma^{(2)}$ and $\gamma^{(3)}$ combined for a three-body configuration and $\gamma^{(2)}$, $\gamma^{(3)}$, $\gamma^{(3)}$, and $\gamma^{(4)}$ combined for a four-body configuration. (The ordinate scale is 8 between two consecutive longer marks.)

that only when this pathway is modeled as a four-body configuration can the 3.8-Å feature be successfully fit and an accurate determination of the distances and angles be obtained.

On the other hand, the structure of the Cu fragment in **2** is less ordered than that in **3** and a large spread in the bond lengths is observed. Therefore, MS contributions are not necessary for a good fit, and some of the distances are less accurately determined when compared to the crystallographic values.

An interesting comparison between the Cu K-edge data for **2** and **3** is the Cu−N(3)−C(1) signal (Figures 9 and 10), which demonstrates again the angle dependence of the MS effects, even though C is a much weaker backscatterer than Fe in the three-body Cu−O/OH−Fe signals.[4] The amplitude enhancement of the EXAFS signal from a bent Cu−N(3)−C(1) configuration (147.3°) to the nearly linear structure (174°) is quite evident. The bent Cu−N(3)−C(1) signal is so weak (Figure 10) that a fit without it did not significantly change the other fitting results.

Overall Results and Statistical Determination of the Bridge Structure. The results from the Fe and Cu K-edge fits show that good agreements with the crystallographic values can be obtained for the data of such complex systems as **2** and **3** (Tables 1 and 2). The Fe fragment is especially complicated; the porphyrin and the pyridine ligands contribute many MS pathways. This makes it impossible (as limited by the dimension of the program and restricted by the number of independent points in the spectra) to include all the necessary signals in the fit, and some of these signals can be strongly correlated with each other. As a result, some of the distances were not well determined. The distances of Fe−N(3) (for both **2** and **3**) and Fe−C(1) (for **3**) were consistently refined to shorter values than observed crystallographically. However, the refined Fe···Cu distance of the linear bridge structure of **2** was remarkably stable, varying less than 0.01 Å over all reasonable fits and giving excellent agreement with the crystallographic value. Overall, the final fit results show that the average deviation from the crystallographic data is 0.03 Å for all distances and 3.6° for all angles determined.

In order to better establish error limits on the bridge parameters, we have applied a statistical analysis methodology[22,27] using two-dimensional contour plots to selected parameters from the multiple-edge fit result for **2**. This analysis

Table 1. Comparison of Selected GNXAS Fit Results[a] with Crystallographic Values for [(py)(OEP)Fe−CN−Cu(Me$_6$tren)]$^{2+}$ (**2**)

structural feature × multiplicity	crystallographic av value[b]	GNXAS distance/angle (bond/angle variance)[c]
Fe−C(1) × 1	1.90 Å	1.89 Å (0.001)
Fe−N(1) × 5	2.01 Å	2.00 Å (0.003)
Fe···C(2) × 10	3.02 Å	3.03 Å (0.004)
Fe···N(3) × 1	3.06 Å	3.01 Å (0.003)
Fe···C(4) × 4	3.40 Å	3.44 Å (0.008)
Fe···C(3) × 8	4.26 Å	4.30 Å (0.005)
Cu−N(3) × 1	1.90 Å	1.93 Å (0.001)
Cu−N(2a) × 1	1.99 Å	1.99 Å (0.005)
Cu−N(2b) × 3	2.14 Å	2.16 Å (0.006)
Cu···C(5) × 6	2.81 Å	2.89 Å (0.009)
Cu···C(6) × 6	3.01 Å	3.06 Å (0.008)
Cu···C(1) × 1	3.02 Å	3.05 Å (0.003)
Fe···Cu × 1	4.94 Å	4.94 Å (0.004)
Fe−C(1)−N(3) × 1	179°	180° (3 × 10^1)
Cu−N(3)−C(1) × 1	174°	180° (4 × 10^0)
Fe−N(1)−C(2) × 10	125.8°	125.9° (6 × 10^0)
Cu−N(2b)−C(6) × 6	112.8°	117.2° (7 × 10^0)

[a] The results shown here are from the multiple-edge fits. [b] Average values of two inequivalent molecules; ref 8. [c] Bond and angle variances are reported in Å^2 and deg^2, respectively.

Table 2. Comparison of Selected GNXAS Fit Results with Crystallographic Values for [(py)(OEP)Fe−CN−Cu(TIM)]$^{2+}$ (**3**)

structural feature × multiplicity	crystallographic av value[a]	GNXAS distance/angle (bond/angle variance)[b]
Fe−C(1) × 1	1.91 Å	1.84 Å (0.002)
Fe−N(1a) × 4	1.97 Å	1.97 Å (0.003)
Fe−N(1b) × 1	2.07 Å	2.03 Å (0.0008)
Fe···C(2a) × 8	3.00 Å	3.00 Å (0.005)
Fe···C(2b) × 2	2.99 Å	2.93 Å (0.01)
Fe···N(3) × 1	3.06 Å	2.94 Å (0.005)
Fe···C(4) × 4	3.37 Å	3.40 Å (0.006)
Fe···C(3) × 8	4.23 Å	4.28 Å (0.005)
Cu−N(3) × 1	2.17 Å	2.14 Å (0.001)
Cu−N(2) × 4	1.97 Å	1.98 Å (0.002)
Cu···C(5) × 4	2.76 Å	2.76 Å (0.003)
Cu···C(6) × 4	3.03 Å	3.07 Å (0.003)
Cu···C(1) × 1	3.20 Å	3.20 Å (0.009)
Cu···C(8) × 2	3.21 Å	3.22 Å (0.01)
Cu···C(7) × 4	4.23 Å	4.24 Å (0.004)
Fe···Cu × 1	5.02 Å	−
Fe−C(1)−N(3) × 1	179°	180° (4 × 10^1)
Cu−N(3)−C(1) × 1	147.3°	153.7° (5 × 10^1)
Fe−N(1a)−C(2a) × 8	126.9°	125.1° (1 × 10^1)
Fe−N(1b)−C(2b) × 2	120.5°	116.5° (3 × 10^1)
Cu−N(2)−C(5) × 4	114.9°	117.3° (3 × 10^0)
Cu−N(2)−C(6) × 4	122.5°	126.1° (2 × 10^0)

[a] Reference 9. [b] Bond and angle variances are reported in Å^2 and deg^2, respectively.

examines correlations among fitting parameters and evaluates statistical errors in the determination of the bridge structure, which will be very useful in cases where the crystallographic data are not available. The approach is described in more detail in ref 4, but in essence parameters with highest correlation dominate in the contribution to the error estimate. The results of **2** are used to illustrate the method because the multiple-edge fitting results included the complete set of bridge parameters.

Figure 11a shows the correlation between the two bond lengths, Fe−C(1) and Cu−N(3). The inner-most contour refers to the 95% error confidence interval. The statistical errors of the two calculated bond distances can be inferred from the plot, which are determined to be ±0.02 Å for both of them. The tilted ellipse indicates that the pair is negatively correlated.

Figure 11b shows the contour plot for the bond lengths of $R_{C(1)−N(3)}$ *vs* $R_{Cu−N(3)}$. A strong statistical correlation between the two is observed, suggesting that the determination of the two distances has large effects on each other. This correlation
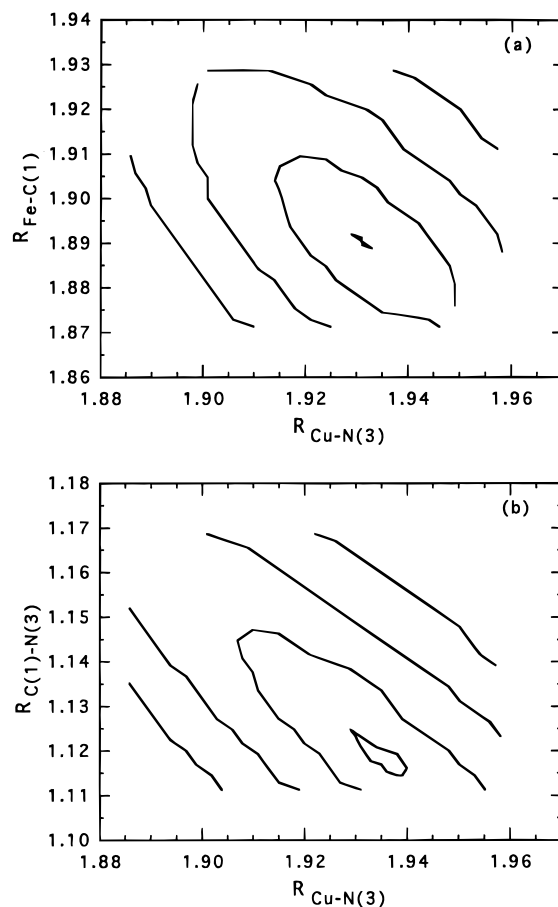

Figure 11. Two-dimensional contour plots for the bridge parameters in the multiple-edge EXAFS fits for **2**: (a) $R_{Fe−C(1)}$ *vs* $R_{Cu−N(3)}$; (b) $R_{C(1)−N(3)}$ *vs* $R_{Cu−N(3)}$. The innermost contour in (a) and the second innermost in (b) correspond to the 95% confidence interval from which the statistical errors are determined.

is also seen between $R_{C(1)−N(3)}$ and $R_{Fe−C(1)}$ (plot not shown). From the plot, the cyanide bond distance $R_{C(1)−N(3)}$ is determined to be 1.12 ± 0.02 Å.

Angle Dependence of Theoretical Four-Body Signals. The angular sensitivity of a MS signal for a three-body configuration has been reported,[20] and it was shown that MS effects become significant at angles above 150°. From the series of the molecular assemblies we have synthesized that contain the Fe−C−N−Cu bridge units, all of them have a virtually linear Fe−C−N fragment, but variations occur with the Cu−N−C angle, from nearly linear to as small as 140°.[33] Thus, we performed a parallel study of the angular dependence of four-body MS effects on the Cu−N−C angle. This was done by calculating a series of theoretical four-body EXAFS signals with a varied Cu−N−C angle from 140° to 180° in increments of 10°. All other parameters were fixed at the crystallographic values of individual complexes.[8] The calculated EXAFS signals were then converted to their corresponding FTs for most effective visual presentation of the results. Figure 12 shows the relative FT magnitude of $\gamma^{(4)}$ as a function of the Cu−N−C angle. A clear trend of increasing FT magnitude as the angle becomes bigger is observed. The FT magnitudes for the signals with an angle of 180° and 170° are relatively close and considerably larger than that for an angle of 160°, whose signal has only about one third of the magnitude of the 180° signal. The MS effects from a Cu−N−C angle of 150° and 140° are even

(33) This angle is found in a trinuclear complex having the bridge unit Fe^{III}−CN−Cu^{II}−NC−Fe^{III},[9] it is currently the lower limit in any bridge containing **1** regardless of the nuclearity of the complex.
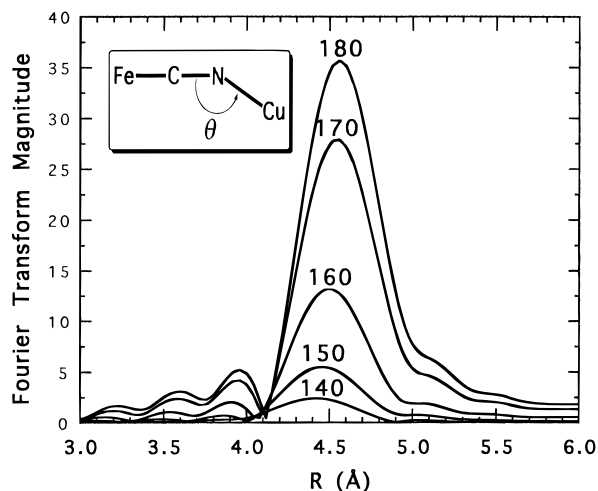
Figure 12. FT magnitudes showing the angular dependence of the EXAFS signal from the Fe−C−N−Cu configuration as a function of the Cu−N−C angle. The significant increase in the FT magnitude for the Cu−N−C angle greater than 160° is evident. (The ordinate scale is arbitrary to show the relative magnitude.)

smaller; their FT magnitudes are only a small fraction of that for 180°. In fact, the $\gamma^{(4)}$ signal at 140° is so weak that it has only half of the strength as that of its corresponding $\gamma^{(2)}$, which remains relatively the same independent of the angle. Because their contributions to the FT are minimal, a signal corresponding to a configuration with an angle less than ∼160° can be ignored in fits and would thus not be detectable, as seen in the case of **3**.

Summary

In this investigation, we have used GNXAS to calculate successfully four-body MS signals for complex inorganic molecular systems. This approach has been applied to two heme-based assemblies containing bridge units **1** which differ significantly in the Cu−N−C angle and the Cu−N distance. A strong long-range Fe−Cu interaction has been observed in **2**, which has a linear four-body bridge. The GNXAS analysis of the Fe and Cu K-edge data of this complex shows that this long-range interaction can be attributed to strong MS effects in the linear bridge, which contributes ∼50% of the intensity of the FT peak at 4.6 Å. On the other hand, no Fe−Cu interaction can be detected for **3** as a result of a bent structure at the Cu end of the bridge.

Theoretical calculations for a four-body Fe−C−N−Cu MS pathway with a varied Cu−N−C angle show that MS effects are sensitive to this angle. A large enhancement of MS intensity occurs for a linear or nearly linear four-body configuration (Figure 12). Any MS effects generated by a configuration with an angle below about 160° do not contribute significantly to the total EXAFS and, therefore, can be ignored. *The angle dependence of MS effects in a four-body configuration demonstrates that it is possible to differentiate a linear and a bent four-body geometry in the outer range of FTs.* A long-range interaction out to ∼5 Å may indicate a linear four-body arrangement. With these experimental and theoretical results, we are in a position to meaningfully examine XAS spectra of cyanide-inhibited heme−copper oxidases. Together with other spectroscopic approaches, we seek, as noted at the outset, to provide a description at a molecular level of detail of cyanide toxicity.